Journal of Non-Crystalline Solids 471 (2017) 274–279

Contents lists available at ScienceDirect

Journal of Non-Crystalline Solids

journal homepage: www.elsevier.com/locate/jnoncrysol

Densification of amorphous boron under pressure

Murat Durandurdu

Department of Materials Science and Nanotechnology Engineering, Abdullah Gül University, Kayseri, 38080, Turkey

ARTICLE INFO

Keywords:
Polyamorphism
Phase transformation
Boron

ABSTRACT

The densification mechanism of amorphous boron under pressure is investigated using a constant pressure *ab initio* technique and found to be associated with two consecutive amorphous-to-amorphous phase transformations. Amorphous boron gradually transforms into a high density amorphous phase, followed by a first order phase transformation into another high density amorphous state. The high density amorphous phases of boron are not quenchable to ambient pressure. Most quasimolecular B_{12} icosahedra in the model are found to be stable at the highest the theoretical pressure of 280 GPa reached in the present work and thus the phase transformations are principally due to the re-structural arrangements in the parts of the model connecting B_{12} icosahedra.

1. Introduction

Boron is an important element because of its superior physical properties and numerous technological applications. Even though it was discovered > 200 years ago, it still stays as the most puzzling element [1,2]. Due to its complex structure, its ground state is still not well established yet. Initially β-rhombohedral (B_{106}) was assigned as the ground state structure because it was frequently perceived in experiments [3–7]. Recent investigations proposed two different phases as a candidate for its ground state structure. The first one is the well-known form of boron, α-rhombohedral (B_{12}) [2]. The second one is a new crystal structure called as τ-B (an orthorhombic structure with the space group of *Cmcm*) having 210 atoms in the unitcell [8]. The quantum mechanical simulations suggest that the τ-B phase is more stable than β-rhombohedral by 13.8 meV/atom and more stable than α-rhombohedral by 9.5 meV/atom [8]. Yet this new crystalline structure has been questioned in later studies [9,10].

Researchers have made considerable efforts to uncover the pressure-temperature phase diagram of boron [11–17]. According to the experimental phase diagram, α-rhombohedral (B_{12}), β-rhombohedral, γ-orthorhombic (B_{28}), δ-tetragonal (B_{50}, T-50 or T52), ε-rhombohedral (B_{15}, isostructural to boron carbide $B_{13}C_2$) can form at ambient and high pressure and temperature conditions. An α-Ga type structure was considered as a candidate for boron above 90 GPa [17]. In addition to these crystalline phases, a pressure-induced amorphization of β-rhombohedral at a high pressure of 100 GPa was reported in an experiment [18]. This amorphous phase was quenchable to ambient pressure.

Amorphous boron (*a*-B) also exists and can be synthesized using different experimental procedures [19–28]. Although the microstructure of *a*-B is assumed to be comparable with that of the crystalline phases, its local structure still remains controversy as well. The β-rhombohedral-like structure [25–27], α-tetrahedral-like configuration [28] and a transition state between α- and β-rhombohedral [24] were suggested for *a*-B. In a recent *ab initio* simulation, a structure comparable to the α-rhombohedral-like phase was projected for *a*-B [29].

An experiment work focused on the high-pressure behavior of *a*-B [11] and *a*-B → α-rhombohedral, *a*-B → β-rhombohedral and *a*-B → δ-tetragonal phase transformations were observed depending on the temperature (1400–1500 K) and pressure (11–15 GPa) conditions applied. To our knowledge, no other research has been performed to better understand its response to high pressure so far. Limited information regarding *a*-B under pressure inspires us to execute this simulation. Here using a constant pressure *ab initio* method, we compress an *a*-B model and find two amorphous to amorphous phase transformations: Amorphous boron transforms progressively to a high-density amorphous (HDA) phase up to 230 GPa at which point it presents a first order phase transformation into another high-density amorphous phase having a mean coordination number of 7.35.

2. Methodology

A density functional theory (DFT) code, SIESTA [30], was used in the present work to investigate the high-pressure behavior of *a*-B. We used the Troullier and Martins scheme to contract pseudopotentials [31] and a generalized gradient approximation (GGA) [32,33] to evaluate the exchange correlation energy. The double zeta basis set was used. The Brillouin zone integration was done at Γ point. The isoenthalpic-isobaric ensemble using the Parrinello-Rahman method [34] and power quenching technique was selected to perform the present simulations. At high-pressures, the model was relaxed using the force

E-mail address: murat.durandurdu@agu.edu.tr.

http://dx.doi.org/10.1016/j.jnoncrysol.2017.06.002
Received 29 March 2017; Received in revised form 21 May 2017; Accepted 5 June 2017
Available online 12 June 2017
0022-3093/ © 2017 Elsevier B.V. All rights reserved.

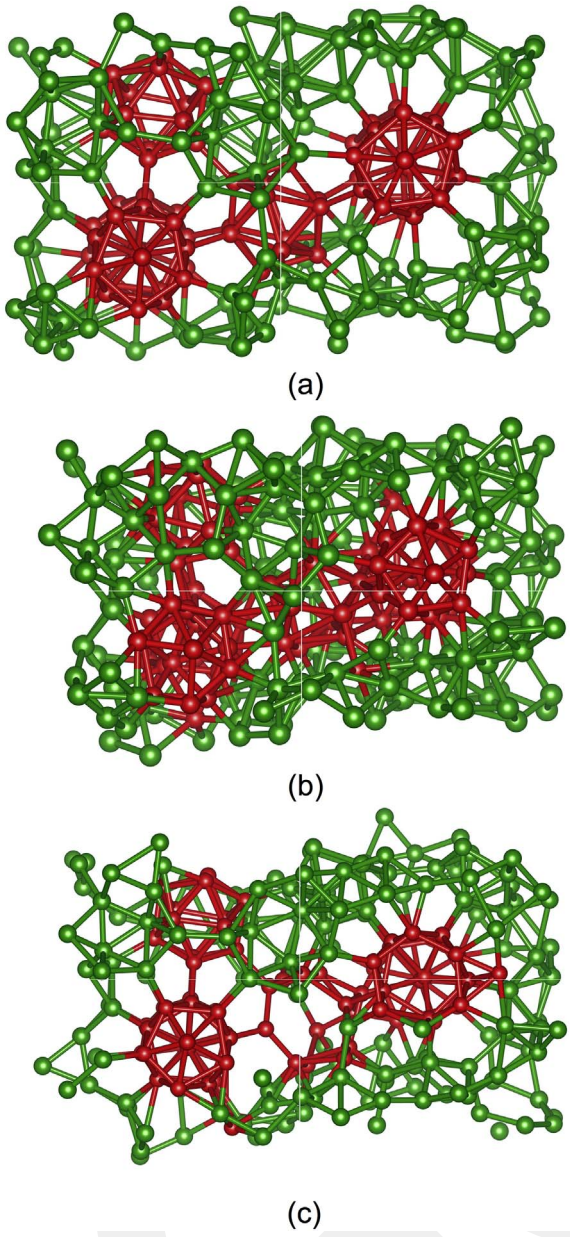

Fig. 1. (a) Uncompressed model (b) VHDA model at 230 GPa (c) Decompressed model. For clarity and to see how the B_{12} icosahedra change under pressure, the atoms of some ideal B_{12} icosahedra in the uncompressed model are represented by a different color.

criteria of 0.01 eV/Å. Some of structural analyses were carried out using the ISAACS [35] and VESTA [36] programs. The amorphous network having 224 atoms was created using the same DFT code and the same simulation parameters in our previous investigation [29] in which the melt and quench method and the isothermal-isobaric ensemble were used.The model mainly consisted of B_{12} icosahedra as shown in Fig. 1 In contrast to the earlier predictions [24–28], however, it was found to be structurally close to the α-rhombohedral boron (see Ref. 29 for more information). The origin of the contradictory observations between the present and previous investigations was attributed to impurities. Namely our model was 100% pure whist the samples used in experiments were not. Note that boron is very sensitive to contaminations and hence it is not easy to have boron samples with negligible amount of impurities in experiments. Consequently we believe that our model represents the local structure of pure *a*-B. Yet careful investigations on the influences of impurities on the local structure of *a*-B will be necessary to clarify this issue.

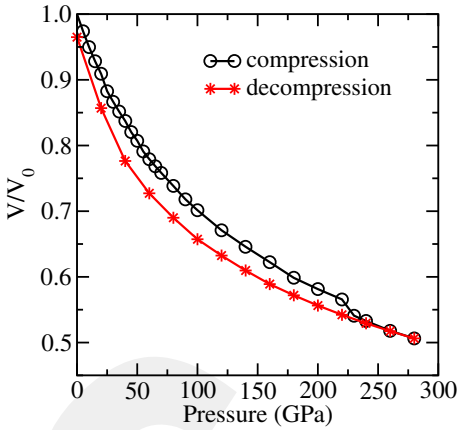

Fig. 2. Variation of volume under pressure.

3. Results

Fig. 2 illustrates the modification of the normalized volume with the application of pressure. The change in the volume is mostly smooth at pressures of up to 230 GPa at which point it shows a small discontinuity. The volume collapse at this pressure is about 5% and might imply a first order-like phase transformation in *a*-B. On pressure release from 280 GPa, a hysteretic behavior is observed but a structure slightly denser than the original one is attained at zero-pressure, demonstrating that a pressure-induced permanent densification in *a*-B is trivially small.

In order to uncover the pressure-induced restructurings in the model, we next probe real space pair correlation functions (PCFs), one of the most commonly used techniques to resolve the structural features of materials at ambient and high pressure and temperature conditions, and present them in Fig. 3. The PCFs exhibit an obvious short-range order and the absence of a long-range order during the entire compression process. This finding reflects the fact that *a*-B still retains its disorder nature at the highest-pressure explored at the present work and experiences amorphous-to-amorphous phase transformation(s).

From the PCFs analysis, we also perceive that the first neighbor separation gradually decreases with increasing pressure and accompanied by the volume collapse at 230 GPa it sharply increases to a larger value as shown in Fig. 4. A sudden enlargement in the mean bond distance is related to the substantial structural rearrangements in the model. Upon decompression, the first neighbor distance continuously increases and reaches the value of the initial model, indicating that the recovered amorphous arrangement is structurally close to the

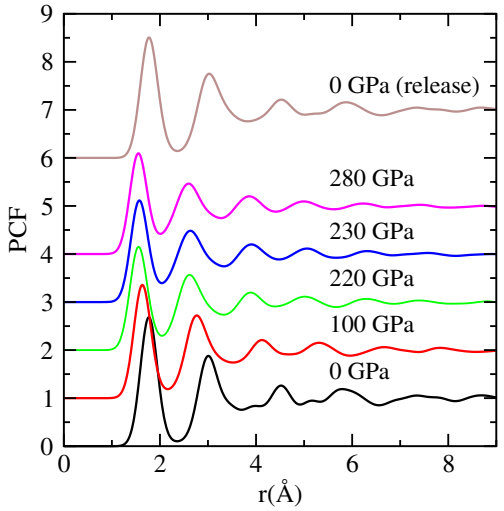

Fig. 3. Pair correlation function (PCF).

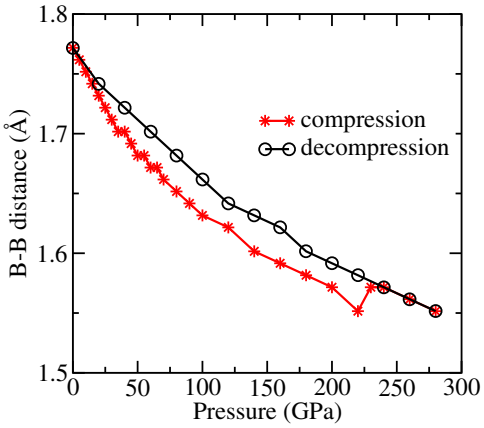

Fig. 4. Modification of the average B-B separation in *a*-B as a function of pressure.

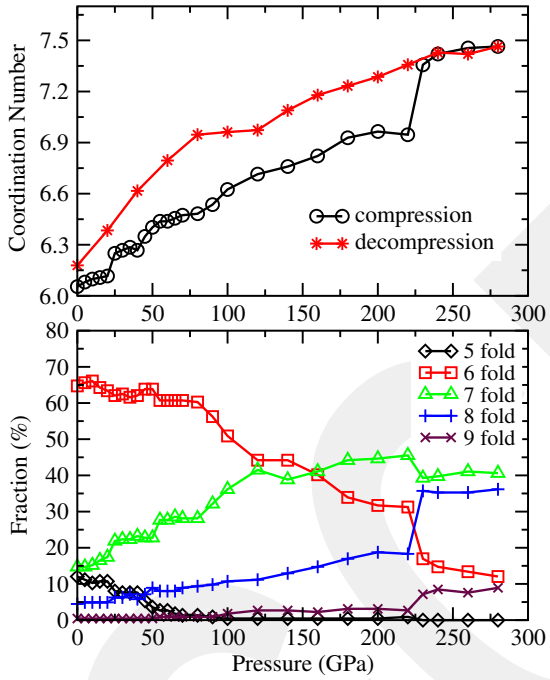

Fig. 5. (a) Mean coordination number and (b) coordination distribution under pressure.

uncompressed network.

Fig. 5 shows the pressure-dependence of the mean coordination number (CN) that is estimated from the first minimum of the PCFs. The cutoffs are determined in the ranges of 2.03–2.36 Å depending on the pressure applied. It should be noted that the CN is very sensitive to the cutoff used and hence we might expect some uncertainty in the projected CN at each applied pressure. At ambient pressure, the average coordination is about 6.1, comparable with the experimental result of 6.3 [37]. With the application of pressure, it gradually increases to ~6.9 at 220 GPa and jumps to a value of 7.35 at 230 GPa. The coordination rise at this pressure is about 6.5%. During the decompression process, the CN decreases continuously and has a value of 6.17 at atmospheric pressure.

In order to gain additional information concerning the local structure of the system, the coordination distribution is investigated at each applied pressure and provided in Fig. 5. At ambient condition, the model principally involves sixfold (65%), sevenfold (15%) and fivefold (13%) coordinated motifs. As the applied pressure is increased, the number of the fivefold coordination decreases and becomes negligible small at around 55 GPa. On the other hand, the fraction of the sixfold configurations remains almost unchanged up to 80 GPa and then drastically decreases but they still persist at 230 GPa with a frequency of 12%. The fraction of the sevenfold-coordinated motifs rises interruptedly and they become the major building units beyond 160 GPa. The amount of the eightfold coordination, on the other hand, increases with some fluctuations up to 230 GPa at which point it rapidly rises to a larger value. The ninefold coordinated clusters with a frequency of 7% also form in the system at 230 GPa. Consequently, the sevenfold (~40%) and eightfold (~36%) motifs are the most privilege clusters above 220 GPa, suggesting that the local structure of the dense amorphous phases beyond 220 GPa predicted in the present study is relatively different than that of known boron crystals because the crystals are mainly structured by the sixfold and/or sevenfold coordinated motifs.

The decompressed amorphous structure essentially entails sixfold (% 59.5), sevenfold (25%) and fivefold (10%) coordinated configurations, revealing striking similarities between decompressed and uncompressed arrangements.

To shed further light onto the structural changes at the atomistic level, we carefully probe the system at each applied pressure using the Voronoi polyhedra approach [38] in which the indices $\langle n_3, n_4, n_5, n_6, \ldots\rangle$ are used to symbolize a Voronoi polyhedron, where n_i and Σn_i donate the number of *i*-edge faces of polyhedron and the CN, correspondingly. At ambient pressure, the *a*-B model shows fourteen different polyhedrons. The most dominated ones and the most affected ones under pressure are given in Fig. 6. All these polyhedra except one having ⟨2, 3, 0, 0⟩ index have one thing in common: they consist of an ideal pentagonal pyramid. Yet their major difference is the CN of the center atom and/or the location/position of the neighboring atom(s) at the top of the central atom. It should be noted that the ⟨2, 3, 0, 0⟩ arrangement correspond to incomplete pentagonal pyramids and the ⟨1, 3, 3, 1⟩ ones involve both the pentagonal and hexagonal pyramids. At ambient condition, the configurations with the ⟨2, 2, 2, 0⟩ and ⟨2, 3, 0, 0⟩ indices are the most popular ones with ~65% and ~12.5% frequencies, respectively. As shown in Fig. 7, their fraction decreases under pressure. At 55 GPa, the ratio of the defective pentagonal pyramids becomes negligible small. The ⟨2, 2, 2, 0⟩ type clusters still preserve and have a frequency of about 12% at 230 GPa. The sevenfold-coordinated configurations are represented by three different Voronoi polyhedrons: ⟨1, 3, 3, 0⟩, ⟨5, 2, 0, 0⟩ and ⟨2, 2, 2, 1⟩ whose portion is ~3.1%, 4.0% and 5.0% at ambient pressure, correspondingly. Under pressure, the percentage of all these polyhedra increases but the formation of ⟨2, 2, 2, 1⟩ type clusters is more favorable than the others. At 230 GPa, the fraction of ⟨1, 3, 3, 0⟩, ⟨5, 2, 0, 0⟩, and ⟨2, 2, 2, 1⟩ is ~11%, 8.5% and 14%, respectively. The eightfold coordinated motifs are characterized by two different polyhedra having the indices of ⟨4, 4, 0, 0⟩ and ⟨1, 3, 3, 1⟩. Both have a tendency to increase gradually up to 230 GPa at which point they exhibit a sudden increase to a larger value (11% and 12%). The Voronoi analysis suggests that the pentagonal pyramids survive in the system at high pressures. Since B_{12} molecules consists of the pentagonal pyramids, one can argue that the B_{12} molecules might persist at high pressure as well. In order to verify this suggestion, we carefully check the B_{12} molecules in the system and find that they are mostly stable with some small deformations and/or defects (see Fig. 1). Thus, we propose that the pressure-induced major structural modifications occur in the parts of model connecting B_{12} molecules. Yet we need to note here that the defective B_{12} molecules formed at high pressures do not fully transform back to the perfect B_{12} molecules upon pressure release (see Fig. 1).

According to the Voronio polyhedra analysis, the decompressed model predominantly consists of the pentagonal pyramids with a frequency of ~53%. Relative to the original amorphous configuration, we find about 11% reductions in the number of the pentagonal pyramids in the decompressed model. The fraction of the incomplete pentagonal pyramids (⟨2, 3, 0, 0⟩) is about 10%. This value is ~2.5% less than that of the initial model. The percentage of the ⟨5, 2, 0, 0⟩ clusters is almost the same in the uncompressed and decompressed networks. On the

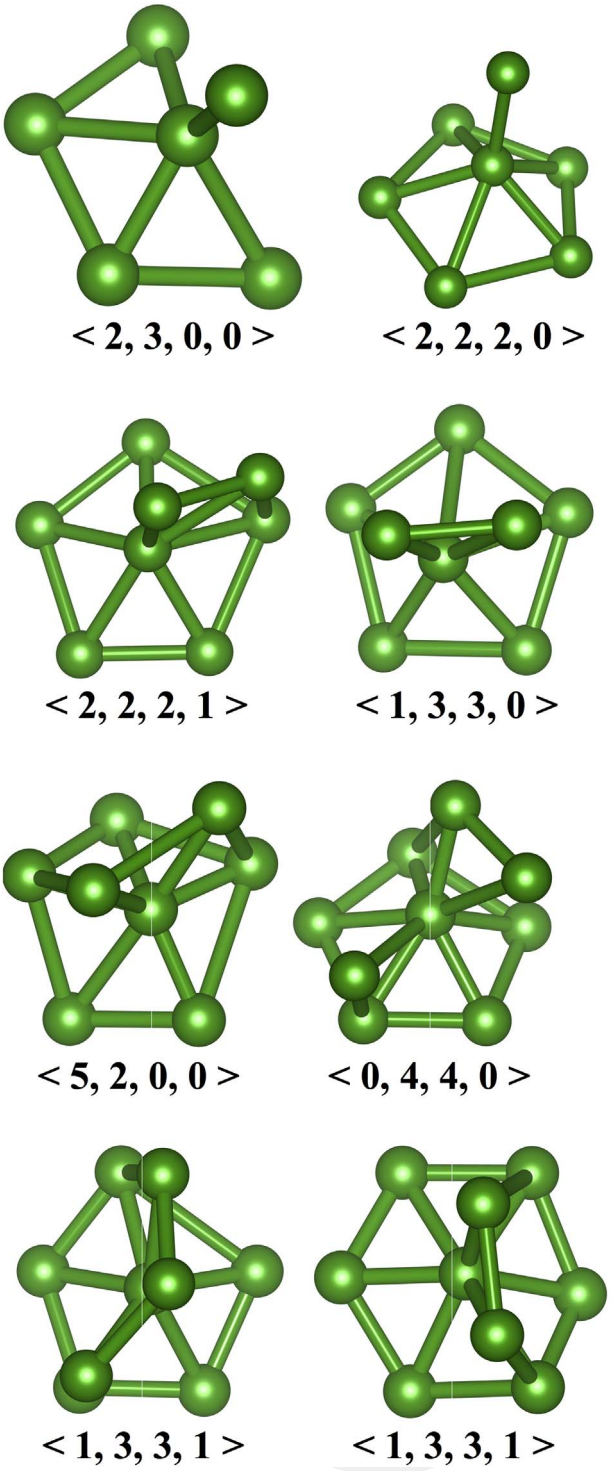

Fig. 6. The most common Voronoi polyhedrons formed in *a*-B at ambient and high pressures.

other hand, we see about 7.5% and 3% increases in the number of the polyhedrons with ⟨2, 2, 2, 1⟩ and ⟨1, 3, 3, 0⟩ indices, respectively in the decompressed configuration. So one can see that some amounts of high-pressure clusters are persevered in the network during the pressure release. Nevertheless, on the basis of the coordination distribution and Voronio polyhedral investigations, we can safely claim that the uncompressed and decompressed models are structurally close to each other.

We lastly analyze the electronic structure of *a*-B under pressure. *a*-B is known as a semiconductor. The experimental band gap energy was

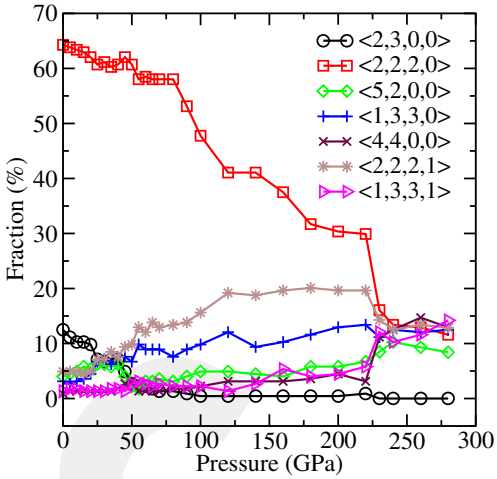

Fig. 7. The change in the Voronoi clusters under pressure.

reported to be in the range from 0.51 eV to 1.0 eV [39–42]. At zero pressure, the HOMO-LUMO band gap is estimated to be 0.27 eV in the present DFT-GGA study. As anticipated, it is less than the experimental values due to the insufficiency of DFT-GGA approach. Because of the small band gap energy, the electron density of states exhibits a semi-metallic-like character as illustrated in Fig. 8. Since DFT-GGA or DFT-LDA simulations generally yield the variation of band gaps under pressure comparable with experiments in spite of their underestimation of the gap energy [43], we also investigate the pressure dependence of the HOMO-LUMO gap width and provide it in Fig. 8 as well. The band gap shows a complex behavior but beyond 80 GPa, the gap has a value larger than that of the ambient pressure model. Subsequently we reach a conclusion that both HDA and VHDA phases carry the characteristic of a semiconductor.

4. Discussion

The structural analyses disclose two possible amorphous-to-amorphous phase transformations in *a*-B. As understood form the pressure

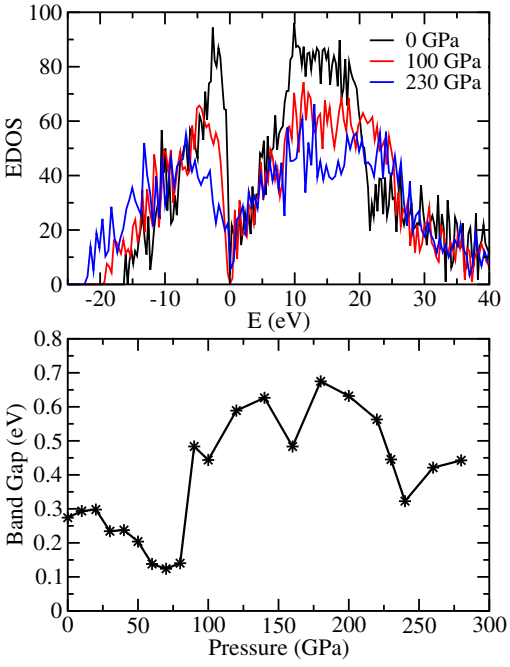

Fig. 8. (a) Electronic density of states and (b) the HOMO-LUMO band gap energy under pressure.

induced modification of volume and CN, the first phase transformation proceeds continuously from a low density amorphous (LDA) state to a HDA up to 230 GPa while the second one seems to be a first order phase change from the HDA phase to very high density amorphous (VHDA) phase. Note that compared to some tetrahedrally coordinated materials, the amorphous-to-amorphous phase transformations in boron do not involve a drastic coordination modification. Indeed the pressure-induced phase transformations in the crystalline boron are not associated with a severe coordination change as well. The CN of the densest crystalline phase of boron (α-Ga) is 7, which is slightly larger than the CNs 6.5–6.6 of the low-pressure phases of boron. Therefore it is quite reasonable to call the phases obtained under pressure as a HDA phase and a VHDA phase.

Note that none of the crystalline phases of boron involves eightfold and ninefold coordinated clusters, and hence the short-range of the VHDA phase is partially different from their local structure. Also among boron phases ever proposed so far, the VHDA phase has the second highest CN after the compressed liquid state having a CN of 8.3 in dynamic shock-compression experiments at a pressure of 100 GPa [44].

One can ask if the mechanism of phase transformations and the topology of the resulting HDA and VHDA phases depend on the initial structure. The answer is yes because our results are based on an amorphous model close to the α-rhombohedral structure but there exists *a*-B, locally parallel to the other crystalline forms of boron, such as β-rhombohedral [25–27], α-tetrahedral [28] or a transition state between these two crystals [24]. They are topologically different than α-rhombohedral and hence at high pressures, each might follow distinct transformation mechanisms and attain amorphous structures different than the HDA and VHDA phases obtained in the present study or transform to a crystalline phase.

Based on the variation of volume, CN, B-B separation, the coordination distribution and Voronio polyhedra investigations on compression and decompression process, we conclude that the phase transformations are reversible in *a*-B. Yet during the decompression process, some high-pressure clusters are persisted in the network, yielding a slightly different amorphous structure compared to the original one. Small distinctions between the uncompressed and decompressed models might be associated with the use of faster rate during the decompression process.

5. Conclusions

The high-pressure behavior of an *a*-B model, structurally similar to the α-rhombohedral boron, is investigated using *ab initio* constant pressure simulations. The incidence of two sequential amorphous-to-amorphous phase transformations is showed through the simulations. The LDA-to-HDA phase transformation proceeds gradually while the HDA-to-VHDA phase change occurs in first order nature. These phase transformations are found to be reversible. Most B_{12} icosahedra persist in both high-density amorphous states and the phase transformations are associated with the structural rearrangements in the areas of the model linking icosahedra.

Acknowledgements

This work was supported by the Scientific and Technological Research Council of Turkey (TÜBİTAK) under grant number 114C100. The simulations were run on the TÜBİTAK ULAKBİM, High Performance and Grid Computing Center (TRUBA resources).

References

[1] A.R. Oganov, V.L. Solozhenko, Boron: a hunt for superhard polymorphs, J. Superhard Mater. 31 (2009) 285.
[2] G. Parakhonskiy, N. Dubrovinskaia, E. Bykova, R. Wirth, L. Dubrovinsky, Experimental pressure-temperature phase diagram of boron: resolving the long-standing enigma, Sci. Rep. 1 (2011) 96.
[3] M.A. White, A.B. Cerqueira, C.A. Whitman, M.B. Johnson, T. Ogitsu, Determination of phase stability of elemental boron, Angew. Chem. 127 (2015) 3697.
[4] S. Shang, Y. Wang, R. Arroyave, Z.K. Liu, Phase stability in α-and β-rhombohedral boron, Phys. Rev. B 75 (2007) (2007) 092101.
[5] L.V. McCarty, J.S. Kasper, F.H. Horn, B.F. Decker, A.E. Newkirk, A new crystalline modification of boron, J. Am. Chem. Soc. 80 (1958) 2592.
[6] T. Ogitsu, F. Gygi, J. Reed, Y. Motome, E. Schwegler, G. Galli, Imperfect crystal and unusual semiconductor: boron, a frustrated element, J. Am. Chem. Soc. 131 (2009) 1903.
[7] D.L. Prasad, M.M. Balakrishnarajan, E.D. Jemmis, Electronic structure and bonding of β-rhombohedral boron using cluster fragment approach, Phys. Rev. B 72 (2005) 195102.
[8] Q. An, K.M. Reddy, K.Y. Xie, K.J. Hemker, W.A. Goddard III, New ground-state crystal structure of elemental boron, Phys. Rev. Lett. 117 (2016) 085501.
[9] T. Ogitsu, V. Lordi, E. Schwegler, M. Widom, Comment on "New Ground-State Crystal Structure of Elemental Boron", Phys. Rev. Lett. 118 (2017) 159601.
[10] H. Werheit, Comment on "new ground-state crystal structure of elemental boron", Phys. Rev. Lett. 118 (2017) 089601.
[11] O.O. Kurakevych, Y. Le Godec, T. Hammouda, C. Goujon, Comparison of solid-state crystallization of boron polymorphs at ambient and high pressures, High Pressure Res. 32 (2012) 30.
[12] V.L. Solozhenko, O.O. Kurakevych, Equilibrium pT phase diagram of boron: experimental study and thermodynamic analysis, Sci. Rep. 3 (2013) (2013) 2351.
[13] A.R. Oganov, Boron under pressure: phase diagram and novel high-pressure phase, Boron Rich Solids, Springer Netherlands, 2010, pp. 207–225.
[14] A.R. Oganov, J. Chen, C. Gatti, Y. Ma, Y. Ma, C.W. Glass, Z. Liu, T. Yu, O.O. Kurakevych, V.L. Solozhenko, Ionic high-pressure form of elemental boron, Nature 457 (2009) 863.
[15] E.Y. Zarechnaya, L. Dubrovinsky, N. Dubrovinskaia, Y. Filinchuk, D. Chernyshov, V. Dmitriev, N. Miyajima, A. El Goresy, H.F. Braun, S. Van Smaalen, I. Kantor, Superhard semiconducting optically transparent high pressure phase of boron, Phys. Rev. Lett. 102 (18) (2009) 185501.
[16] K. Shirai, A. Masago, H. Katayama-Yoshida, High-pressure properties and phase diagram of boron, Phys. Status Solidi B 244 (303) (2007).
[17] U. Häussermann, S.I. Simak, R. Ahuja, B. Johansson, Metal-nonmetal transition in the boron group elements, Phys. Rev. Lett. 90 (2003) (2003) 065701.
[18] D.N. Sanz, P. Loubeyre, M. Mezouar, Equation of state and pressure induced amorphization of β-boron from X-ray measurements up to 100 GPa, Phys. Rev. Lett. 89 (2002) 245501.
[19] L. Vandenbulcke, G. Vuillard, Chemical vapor deposition of amorphous boron on massive substrates, J. Electrochem. Soc. 123 (1976) 278.
[20] K. Shirai, S.I. Gonda, Characterization of hydrogenated amorphous boron films prepared by electron cyclotron resonance plasma chemical vapor deposition method, J. Appl. Phys. 67 (1990) 6286.
[21] K. Nakamura, Preparation and properties of amorphous boron films deposited by pyrolysis of decaborane in the molecular flow region, J. Electrochem. Soc. 131 (1984) 2691.
[22] F. Galasso, R. Vaslet, J. Pinto, Formation of amorphous boron from the melt by rapid cooling, Appl. Phys. Lett. 8 (1966) 331.
[23] K. Katada, An electron diffraction study evaporated boron films, Jpn. J. Appl. Phys. 5 (1966) 582.
[24] A.R. Badzian, Radial distribution function of non-crystalline boron, Mater. Res. Bull. 2 (1967) 987.
[25] M. Kobayashi, Structure of amorphous boron, J. Mater. Sci. 23 (1988) 4392.
[26] R.G. Delaplane, U. Dahlborg, W.S. Howells, T. Lundström, A neutron diffraction study of amorphous boron using a pulsed source, J. Non-Cryst. Solids 106 (1988) 66.
[27] J.S. Gillespie Jr., Crystallization of massive amorphous boron, J. Am. Chem. Soc. 88 (1966) 2423.
[28] Y.G. Poltavtsev, V.P. Zakharov, V.M. Pozdnyakova, Electron diffraction studies of carbon and boron amorphous films, Kristallografiya 18 (1973) 425.
[29] M. Durandurdu, Liquid boron and amorphous boron: an ab initio molecular dynamics study, J. Non-Cryst. Solids 417 (10) (2015).
[30] P. Ordejón, E. Artacho, J.M. Soler, Self-consistent order-N density-functional calculations for very large systems, Phys. Rev. B 53 (1996) R10441.
[31] N. Roullier, J.L. Martins, Efficient pseudopotentials for plane-wave calculations, Phys. Rev. B 43 (1991) 1993.
[32] A.D. Becke, Density-functional exchange-energy approximation with correct asymptotic behavior, Phys. Rev. A 38 (1988) 3098.
[33] C. Lee, W. Yang, R.G. Parr, Development of the Colle-Salvetti correlation-energy formula into a functional of the electron density, Phys. Rev. B 37 (1988) 785.
[34] M. Parrinello, A. Rahman, Crystal structure and pair potentials: a molecular-dynamics study, Phys. Rev. Lett. 45 (1980) 1196.
[35] S. Le Roux, V. Petkov, ISAACS–interactive structure analysis of amorphous and crystalline systems, J. Appl. Crystallogr. 43 (2010) 81.
[36] K. Momma, F. Izumi, VESTA 3 for three-dimensional visualization of crystal, volumetric and morphology data, J. Appl. Crystallogr. 44 (2011) 1272.
[37] R.G. Delaplane, R. G., T. Lundstrom, U. Dahlborg, W.S. Howells, D. Emin, T.L. Aselage, A.C. Switendick, B. Morosin, C.L. Beckel (Eds.), Boron-Rich Solids, AIP Conf. Proc., No. 231, AIP, New York, 1991(p. 241).
[38] N.N. Medvedev, The algorithm for three-dimensional voronoi polyhedral, J. Comput. Phys. 67 (1986) 223.
[39] A. Hori, M. Takeda, H. Yamashita, K. Kimura, Absorption edge spectra of boron-rich amorphous films constructed with icosahedral cluster, J. Phys. Soc. Jpn. 64 (1995) 3496.

[40] K. Kimura, T. Tada, A. Hori, A. Furukawa, Optical absorption edge and photoluminescence spectra in amorphous and crystalline boron-rich solids, J. Non-Cryst. Solids 137 (1991) 919.
[41] A.A. Berezin, O.A. Golikova, M.M. Kazanin, T. Khomidov, D.N. Mirlin, A.V. Petrov, A.S. Umarov, V.K. Zaitsev, Electrical and optical properties of amorphous boron and amorphous concept for ß-rhombohedral boron, J. Non-Cryst. Solids 16 (1974) 237.
[42] U. Kuhlmann, H. Werheit, T. Lundström, W. Robers, Optical properties of amorphous boron, J. Phys. Chem. Solids 55 (1994) 579.
[43] F.J. Manjón, D. Errandonea, A. Segura, V. Muñoz, G. Tobías, P. Ordejón, E. Canadell, Experimental and theoretical study of band structure of InSe and In 1 − x Ga × Se (x < 0.2) under high pressure: direct to indirect crossovers, Phys. Rev. B 63 (2001) 125330.
[44] S. Le Pape, A.A. Correa, C. Fortmann, P. Neumayer, T. Döppner, P. Davis, T. Ma, L. Divol, K.U. Plagemann, E. Schwegler, R. Redmer, Structure measurements of compressed liquid boron at megabar pressures, New J. Phys. 15 (2013) 085011.

GCRIS